ABSTRACT

Title of dissertation: THE SMALL MECHANOSENSITIVE CHANNEL: ADAPTIVE GATING AND TIMING DURING HYPOOSMOTIC SHOCK.

Miriam Sara Boer, Doctor of Philosophy, 2011

Dissertation directed by: Prof. Sergei Sukharev, Dept. of Biology

Mechanosensation is the ability to respond to mechanical stimuli. It is present in many organisms. In *Escherichia coli* (*E. coli*), mechanosensation manifests in two membrane channels, the large mechanosensitive channel (MscL) and the small mechanosensitive channel (MscS). Both osmoregulatory channels sense membrane tension. MscS, the subject of these studies, consists of a transmembrane region and a cytoplasmic cage. It opens at tensions below those which can cause immediate damage to membranes, contrasting with MscL which opens at near-lytic tensions. Because it opens at non-threatening tensions, MscS not only opens and closes but also inactivates. Inactivation is non-conductive and tension insensitive, and this adaptive behavior was first observed on patch clamp. With the aid of carefully constructed molecular models, the first part of this dissertation evaluates whether inactivation is merely a patch clamp

artifact or if it is indeed a part of *in vivo* MscS function. Working with wild type (WT) alongside fast inactivating and noninactivating mutants proved inactivation does confer a survival advantage to hypoosmotically shocked bacteria. Additionally, light scattering was used to view the swelling and channel response events in WT and knock out (KO) cells lacking mechanosensitive channels upon instantaneous hypoosmotic shock by way of stopped flow.

THE SMALL MECHANOSENSITIVE CHANNEL: ADAPTIVE GATING AND TIMING DURING HYPOOSMOTIC SHOCK.

by

Miriam Sara Boer

Dissertation submitted to the Faculty of the Graduate School of the
University of Maryland, College Park in partial fulfillment
of the requirements for the degree of
Doctor of Philosophy
2011

Advisory Committee:

Professor Sergei Sukharev, Chair
Professor Neil Blough
Professor Marco Colombini
Professor Lyle Isaacs
Professor Richard Payne

Acknowledgements

I would like to acknowledge the time my adviser, Prof. Sergei Sukharev, spent and the patience with which he oversaw my progression through the biochemistry program. Without his contributions, I would not be where I am today. Additionally, my advisory committee's diverse perspectives contributed greatly to my development both as a scientist and a person. I will certainly be taking the lessons I learned here to heart and applying them both in lab and life in general.

Also, I would like to acknowledge the support of my family and friends; my parents for making me do my homework when all I wanted was to be the next Lisa Leslie, my grandma and grandpa for being examples of living life on only your own terms, my brother for not literally killing me when he got taller than me after I spent the first couple years of his life tripping him and laughing when he fell as he learned to walk, and all the other incredible family members and great friends who have always talked me up when I've been down. I would like to acknowledge Mr. Martin Rafson, my high school math teacher, and Mr. Ronald Mason, my first fencing coach. Both men taught me to trust my motivation, abilities, instincts, and endurance, intellectually and athletically.

Last, but in no way least, I'd like to acknowledge the efforts of one Dr. Danny Rogers. His contributions to my life as a New York transplant in Maryland have been immeasurable and beyond appreciated.

Table of Contents

List of Figures

Abbreviations:

MscS – mechanosensitive channel of small conductance

MscL – mechanosensitive channel of large conductance

LB – Luria Bertani medium

HEPES – 4-(2-hydroxyethyl)-1-piperazineethanesulfonic acid

HSPC – high speed pressure clamp apparatus

WT – wild type

KO – knock out

Chapter 1

Introduction

Mechanosensation and osmoregulation.

Mechanosensation is the ability of an organism to respond to a given mechanical stimulus, such as hair cells within the ear being sensitive enough to detect sound waves or a bacterium's reaction to membrane stretching caused by osmotic swelling (*3-5*). Mechanosensitive channels are present in many organisms, ranging from excitable animal cells to walled cells in plants and bacteria. Mechanosensitive channels are present as cation selective channels in pectoral muscle cells(*6*) as well as turgor regulators in plants. Several types of eukaryotic channels have been cloned and observed on patch clamp, but their structures are as yet undefined. Several examples are TRPY1 in yeast (*7*), mammalian TRPV4(*8*), two-pore domain K+ channels TREK and TRAAK(*9*), and cation channels piezo1 and piezo2(*10*). In prokaryotic bacteria, mechanosensitive channels may rescue cells from hypoosmotic shock, as observed in *Escherichia coli* (*E. coli*), the model organism discussed in this document. MscL was the first bacterial mechanosensitive channel to be isolated, cloned, and structurally characterized(*2;11*), followed by MscS(*12*). Both crystal structures offer starting points to analyze the channels' mechanisms. MscL, a homopentamer with 3 nS conductance and an in-plane area change of ~20 nm^2 (*13*), opens at near-lytic tensions (9-15 mN/m). Although MscL shows some adaptation in excised patches (*14*), it does not inactivate and exhibits steady activity under constant tension above the threshold. MscS, a homoheptamer with an in-

plane area change of approximately 10.5-15 nm^2 (*14;15*) (Boer, et al, in press), conducts at 1 nS, and opens under moderate sub-lytic tensions (5-8 mN/m) (*14;16;17*). The thermodynamic analysis of patch clamp traces was done according to two-state Boltzmann equation $Po = 1/(1+\exp((\Delta E-\gamma\Delta A)/kT)$, where ΔE and ΔA are the changes in free energy and in-plane area of the protein associated with the opening transition, k is the Boltzmann constant and T absolute temperature. The partial area changes between the closed (C) and open (O) conformations and the transition barrier (B) can be estimated from the tension dependencies for the opening and closing rates: $\Delta A_{C\rightarrow B} = kT\cdot d\ln(k_{on})/d\gamma$ and $\Delta A_{O\rightarrow B} = kT\cdot d\ln(k_{off})/d\gamma$ (*18*).

Bacterial osmoregulation in *E. coli* is a simpler model of mechanosensation, and it is studied for several reasons; *E. coli* are easily observed subjects of osmotic viability assays, the crystal structures of the proteins involved are known, and they are robust patch clamp specimens (*19;19;20*). In *E. coli*, osmotic swelling may occur in natural environments in a variety of situations. For example, if enteric *E. coli* bacteria are expelled when an animal relieves itself, they are initially in a relatively high osmotic environment. If it begins to rain, then the bacteria will be subjected to an osmotic downshock to which they must adapt if they are to survive. Free-living and enteric bacteria possess adaptive mechanisms to survive drastic environmental osmotic changes. Under high osmolarity, bacteria initially accumulate K+, followed by replacement of ions with compatible organic osmolytes (for example, proline, betaine, and trehalose) (*21;22*). When the external osmolarity suddenly drops and water rushes into the cells, bacteria regulate the increased turgor and volume by releasing excessive osmolytes through

mechanosensitive channels. Four known channels regulate the system: the mechanosensitive channel of miniconductance (MscM) (*23*), the potassium-dependent mechanosensitive channel (MscK)(*24*), the mechanosensitive channel of small conductance (MscS), and the large mechanosensitive channel (MscL) (*25-27*). Out of these four, MscS and MscL appear to regulate the bulk of turgor-driven solute release. If either MscS or MscL alone is present in the cell membrane, cells easily survive abrupt osmotic downshock (*12*). Both channels are gated by tension in the lipid bilayer, although they are structurally unrelated (*11;16;28*) **(fig.1.1)**

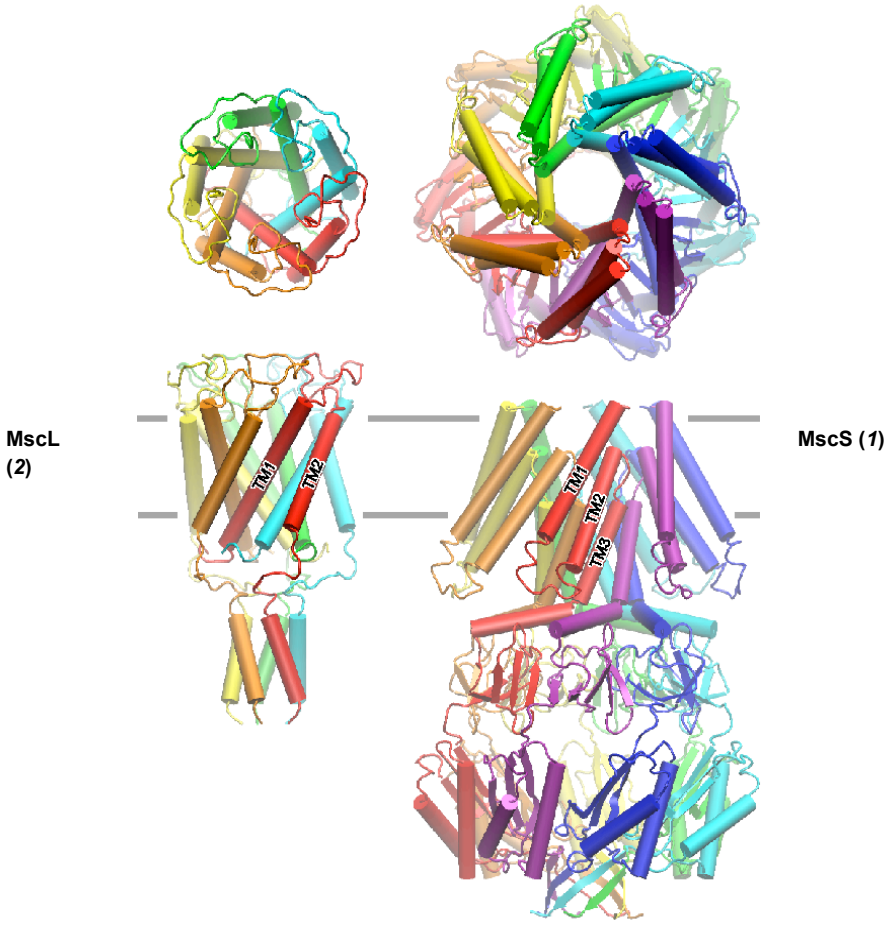

Fig. 1.1 Crystal structures of MscL and MscS. Top: View from the extracellular side perpendicular to the axis of symmetry, Bottom: View parallel to the axis of symmetry. In MscS, TM1, TM2, and TM3 are

labeled, and the kink characteristic of the inactive state is present at G113 (the TM3s straighten in the open state and kink at G121 in the closed resting state). The cage is the portion below the kink in TM3

In excised patches, MscS does not show sustained activity at constant tension; it shows transient adaptive responses which result in complete inactivation. It appears to mediate most turgor-limiting osmolyte exchange under non-lytic conditions. In many 'wild-type' *Escherichia coli* strains, MscL is constitutively produced at the level of 5-10 copies per cell, but MscS can be 2-5 times more abundant. Both genes, *yggB* (*mscS*) and *mscL* are under control of RpoS (σs), a stress-mediating transcription factor (*29*). Both MscS and MscL are large and essentially non-selective channels, so every opening event dissipates vital gradients and comes at a metabolic cost. In contrast to MscL, MscS' transient responses resulting in the inactivated state likely prevent leaks under sub-lytic tension. This adaptive behavior is evident when pressure is applied gradually, and only a fraction of the MscS population opens in contrast to full-scale responses from abrupt transmembrane pressure steps (*15;30*). Both activation and inactivation are triggered by membrane tension with approximately the same threshold but different kinetics (*15*), usually allowing the channel to open first and then gradually inactivate under persisting moderate tension. While the existing crystal structures of WT (*31*) and A106V (*32*) MscS provide starting points for the modeling of the MscS's transitions assisted by EPR (*33;34*) or new computational techniques (*35;36*), detailed functional analysis of opening and inactivation (*30;37*) remains an indispensable part of our understanding of the MscS gating cycle and its structural underpinning.

MscS structure.

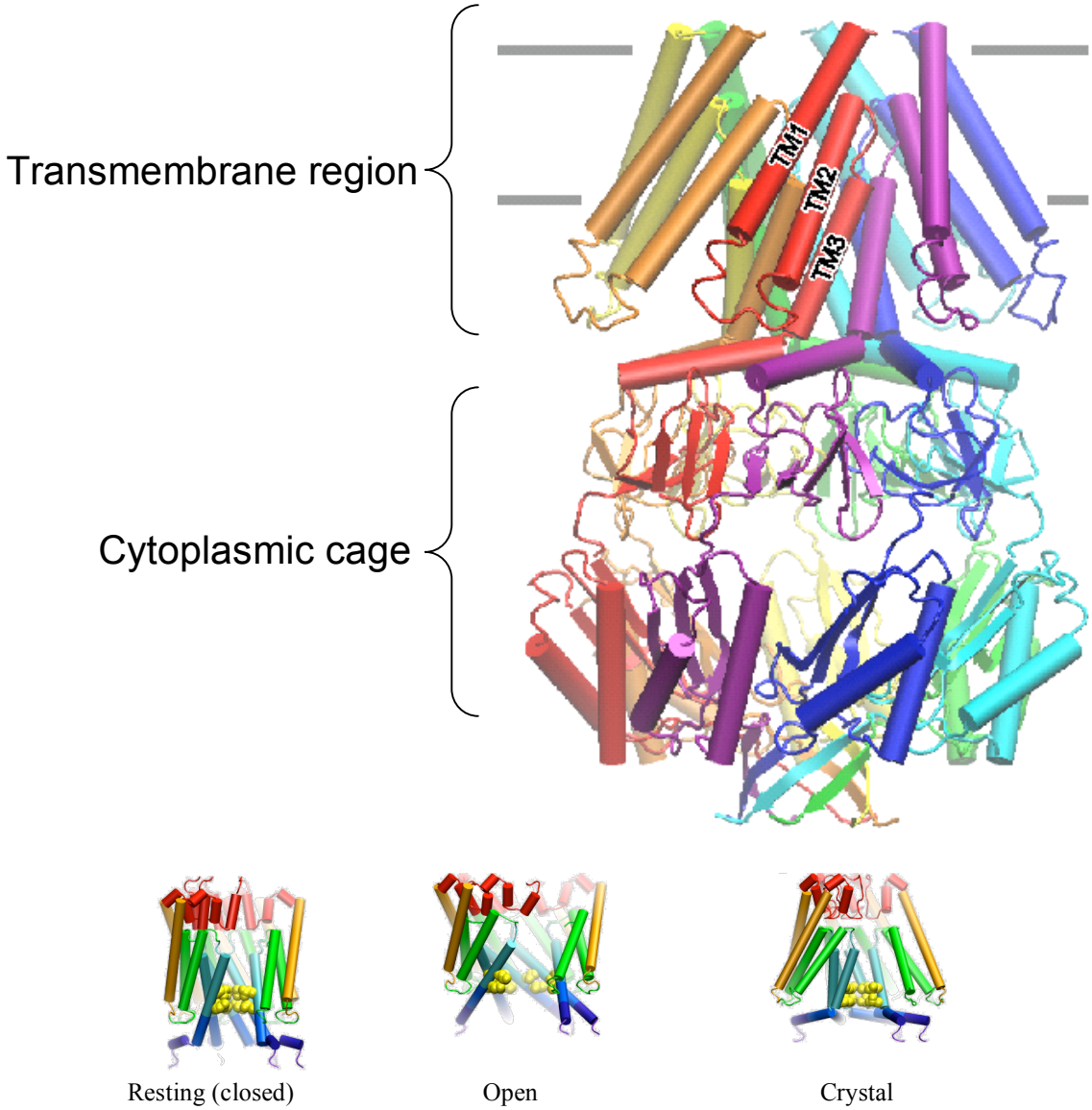

Fig. 1.2 Above, the MscS crystal structure(*1*) with the transmembrane domain and the cytoplasmic cage labeled. Additionally, the TM1, TM2, and TM3 are denoted. Below, the molecular models for the resting or closed state, the open state, and again the crystal structure. In the closed state, there is a characteristic kink at G121. When MscS opens, it is believed that the kink vanishes as the TM3s straighten, and in the crystal structure, the kink is at the G113 residue.

MscS' crystal structure was solved to 3.9 Å (*1*) (**fig. 1.2**). It is a homoheptamer, and each subunit possesses three transmembrane (TM) helices. TM1 and TM2 form a paddle-like structure constituting the protein-lipid interface. TM3 forms both the

hydrophobic pore with the top portion of the helix, and it forms the top of a large hollow cytoplasmic domain, the cage with the lower portion (*1;31*). The crystal structure showed a 30^{o} splay of TM1 and TM2 relative to the pore axis, possibly a result of delipidation. Essentially parallel TM3 helices form the transmembrane pore, kinking sharply at glycine 121 (G121) when closed in the closed model and at G113 in the crystal structure, which we believe to be in some ways representative of the inactive state. It was initially thought to be representative of the open state(*1*), but that may not be the case(*38*). The portion of TM3 below the G113 kink forms the top of the cage. The large hollow cage has seven ports surrounded by charged residues connecting the pore to the cytoplasm. (**fig. 1.2**). Additionally, the diameter of the pore in the crystal structure is too small to maintain the experimentally observed open-state conductance of 1 nS and the TM2-TM3 contacts necessary for tensions transmission from the membrane to the pore are not present (*39;40*). Because the crystal state is nonconductive and there is a sharp kink at G113, it is unlikely to be either the resting or open state, which is why it may represent the inactive state. Using the crystal structure as an initial conformation, the work of the Sukharev group transformed the crystal structure into a compact resting state more capable of responding to membrane tension(*41*). Adding a de-novo modeled N-terminus to MscS (26 amino acids on the periplasmic side) repositioned the channel in the bilayer. Dr. Andriy Anishkin compacted the complex by aligning the TM1-TM2 along TM3s (decreasing TM1-TM2 splay) in vacuum using the new extrapolated motion protocol based on cycles of small displacements and energy minimizations[29]. Modifying the crystal structure thusly led to a more functional and stable protein within the membrane. Relocating the crystallographic kink at G113 two helical turns down the

TM3 to the highly conserved G121 also alleviated steric clash between the TM1-TM2 loops and TM3b.

A stable resting-state model of MscS resulted from these modifications. A plausible pathway for the channel to move from closed to open and back was again envisioned through the extrapolated motion protocol[30]. Starting with the compact resting state, the protocol generated several expansion trajectories. The limits of transition were chosen using experimentally determined conductance and in-plane protein area change. The thermodynamic analysis of patch clamp traces was done as discussed above. The change in area(*15*) was used by Dr. Anishkin as a constraint. The conformation chosen as a likely candidate for the open state was then equilibrated in an all-atom MD simulation which yielded a stable open state model. The overall transition resulted in a 1 nm pore diameter increase and a 12 nm^2 total in-plane expansion of the transmembrane domain. The TM3 helices tilted roughly 10^o relative to their initial placement and kink-free. An additional 56^o rotation of the straightened TM3 helices was observed during MD equilibration making the pore lining more polar, thus stabilizing hydration.

In this open conformation, TM3s appear to work as "struts" for the open pore frame. To return to a nonconducting state, the TM3 helices must re-kink. G121 and G113's flexibility within TM3 demonstrates kinking at G121 is necessary to leave the open state. A G113 kink, however, is requisite for achieving inactivation. Mutant G113A prevents inactivation, and the G121A mutant impedes closing (*30*). The re-coupled TM2 and TM3 helices from the computer-generated resting state revealed a buried hydrophobic contact between them, which apparently works as a force-transmission route from the protein-lipid interface to the gate. Preliminary data show

hydrophilic substitutions in the TM2-TM3 contact predispose the channel to rapid, or "silent," inactivation under sub-threshold tensions directly from the closed state. The question of how the G113 kink may help WT TM2 helices disengage from the gating TM3 helices is a subject of ongoing study. Finally, most MscS modeling focused on the transmembrane domain, generally viewing the cytoplasmic cage as a filter. While there is data suggesting the cage may be sensitive to crowding agents (*42*), more recent data has proven the beta domain, which is part of the cage, to play a large role in overall channel function(*43*). Future efforts may be dedicated towards accurately modeling the cage.

MscS function.

In concise terms, MscS is in a resting nonconductive state when tension is absent. When tension is applied, it may either enter an open or, depending on the degree and manner of tension application, a tension insensitive inactive state(*30*). The relative positions of the activation and inactivation curves define the degree of inactivation. If the activation curve is shifted to the left, then the channels are more likely to open than inactivate. If the activation curve for a particular mutant is shifted to the right, then the channels are more likely to inactivate, and silent inactivation (inactivation without opening) becomes more pronounced(*44*). If the channel does open, it may then either enter a resting nonconductive state or the tension insensitive inactive state. Once inactivated, channels will gradually return to a closed resting state. This can be observed from patch clamp data, which also shows the patch response decrease with a sustained step. Previously referred to as desensitization(*15*), it is now referred to as adaptation and

thought to be a redistribution of tension as the inner membrane leaflet of a given patch slips under sustained tension(*14*). Adaptation is only visible in excised patches on patch clamp, not whole cell experiments. Inactivation prevents MscS from responding to further tension stimuli. (**Fig. 1.3**)

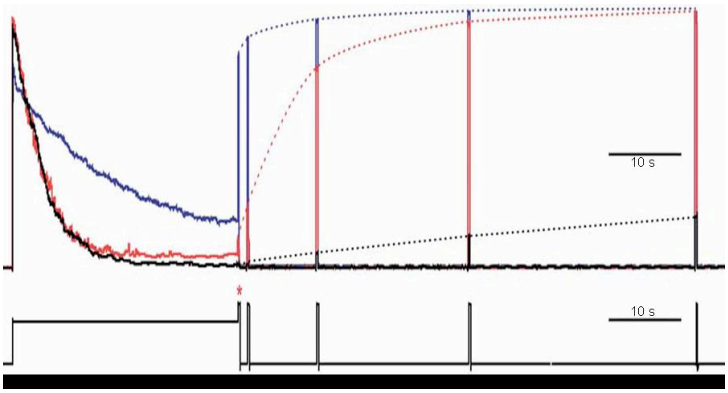

WT: red trace.
G113A: blue trace.
Q112G: black trace.(***30***)

Fig. 1.3 Patch clamp data for MscS WT (red), noninactivating mutant G113A (blue), and a fast inactivator Q112G (black)(***30***). The pressure protocol used is shown below. From this data, we see the initial opening response of the patch to tension and how the signal drops. This drop is adaptation, most likely a result of tension redistribution in the inner membrane leaflet of the lipid bilayer(*14*). We can gauge the degree of inactivation brought on by a given stimulus by pulsing the patch at the end, as was done here (the asterisk denotes that initial pulse). The channels that do not respond are inactive. Additionally, this particular protocol shows us how long before patch conductance returns to its initial level. In contrast to WT, G113A demonstrates a decreased tendency to inactivate, and Q112G demonstrates an increased tendency to inactivate.

The biological question is whether and how inactivation gives an adaptive edge to bacteria subject to short, prolonged, or gradual osmotic challenges. To increase our understanding of the mechanisms of bacterial mechanosensation, one must not only study theoretical modeling and *in situ* patch clamp data but also view the intact system *in vivo*. The first set of studies presented addresses the role of inactivation in the context of both *in vivo* and *in vitro* experiments and the timing of channel activation *in vivo*.

If bacteria adapted to a high-osmotic environment are suddenly osmotically downshocked, they swell. The swelling generates tension in the membrane, and when it

reaches MscS' activation threshold, the channel opens spilling osmolytes into the environment. The tension is relieved, and the cell saves itself from lysis. However, should tension persist at a near-threshold level, inactivation may prevent MscS from opening repeatedly. Repeated opening can pose a serious threat to metabolic gradients. As briefly discussed above, MscS does indeed exhibit transient activity. A cell lacking inactivating channels may initially save itself from rupture only to die perhaps because, for example, it dissipated its proton gradient, thereby losing the ability to produce ATP. To compensate, MscS exhibits inactivation (**fig. 1.3**). The inactivated state, first revealed in patch-clamp experiments, is of particular importance at tensions between those at which MscS opens and the near-lytic tension when MscL opens. Inactivation provides a means of closing and disengaging the channel once the immediate lytic danger passes. This information suggests a sudden *in vivo* downshock will force wild type (WT) MscS to respond and then enter the tension-insensitive inactivated state, preserving membrane integrity and cell viability.

Overall, while MscS is a relatively well-understood model of mechanosensation in *E. coli*, I attempted to add to the existing body of knowledge. There currently exists no data on the relationships between *in vivo* bacterial swelling time and the kinetics of opening, closing, and inactivation. Additionally, there is no data on the survival in osmotic regimes other than straight shock, and there is no evidence for the role of inactivation *in vivo*.

My project included establishing a relationship between MscS' functional cycle determined by patch-clamp and cell physiology that may support the data discussed above. In addition to knock-out (KO) bacterial strains lacking all mechanosensitive

channels, which are osmotically hypersensitive (*12*), we have fast-inactivating and non-inactivating MscS mutants, providing a foundation for *in vivo* experiments exploring the role of inactivation in *E. coli* osmotic survival. Along with WT channels, we evaluated a model noninactivating mutant, G113A, and a model fast inactivating mutant, D62N, to see if patch clamp phenotypes were consistent with *in vivo* behavior. The G113A mutation was intended to remove the flexible glycine from the proposed kink necessary in the TM3s to enable inactivation. D62N was a model fast inactivator, most likely because removing the negatively charged D residue disrupted the modeled salt bridge between the D62 and R131 residues. Both mutants were profiled with *in vivo* assays designed to tax both appropriately dysfunctional channel types so the effect of these abnormalities on cell survival could be evaluated via plating. Additionally, this first part of my research included an attempt to time the swelling and resultant channel activation *in vivo* via light scattering.

Chapter 2

Biochemistry 2011, in press

Adaptive MscS gating in the osmotic permeability response in *E. coli*: the question of time

Miriam Boer, Andriy Anishkin and Sergei Sukharev*

Department of Biology, University of Maryland, College Park, MD 20742

*To whom correspondence should be addressed: Department of Biology, Bldg 144, University of Maryland, College Park, MD 20742, e-mail: sukharev@umd.edu, phone: 301-405-6923
fax: 301-314-9358

TITLE RUNNING HEAD
Timing of MscS activation and inactivation in vivo

The work was supported by the NIH R01GM075225 grant to SS

Abbreviations:

MscS – mechanosensitive channel of small conductance

MscL – mechanosensitive channel of large conductance

LB – Luria Bertani medium

HEPES – 4-(2-hydroxyethyl)-1-piperazineethanesulfonic acid

HSPC – high speed pressure clamp apparatus

ABSTRACT: Microorganisms adapt to osmotic downshifts by releasing small osmolytes through mechanosensitive (MS) channels. We want to understand how the small mechanosensitive channel's (MscS) activation and inactivation, both driven by membrane tension, optimize survival in varying hypoosmotic shock situations. By measuring light scattering with a stopped-flow device, we estimate bacterial swelling time as 30-50 ms. A partial solute equilibration follows within 150-200 ms, during which optical responses from cells with WT MscS deviate from those lacking MS channels. MscS opening rates estimated in patch-clamp show the channels readily respond to tensions below the lytic limit with a time course faster than 20 ms and close promptly upon tension release. To address the role of the tension-insensitive inactivated state *in vivo*, we applied short, long and two-step osmotic shock protocols to WT, noninactivating G113A and fast-inactivating D62N mutants. WT and G113A showed a comparable survival in short 1 min 800 mOsm downshock experiments, but G113A was at a disadvantage under a long 60 min shock. Pre-shocking cells carrying WT MscS for 15 s to 15 minutes with a 200 mOsm downshift did not sensitize them to the final 500 mOsm drop in osmolarity of the second step. However, these two-step shocks induced death in D62N more than just a one-step 700 mOsm downshift. We conclude MscS is able to activate and exude osmolytes faster than lytic pressure builds inside the cell under abrupt shock. During prolonged shocks, gradual inactivation prevents continuous channel activity and assists recovery. Slow kinetics of inactivation in WT MscS ensures that mild shocks do not inactivate the entire population, leaving some protection should conditions worsen.

INTRODUCTION

Previously, most osmotic shock viability tests were performed on cultures pre-equilibrated in high-osmotic media by rapidly mixing them with low osmolarity media and plating them on agar plates within 1-5 min (*12;45*). This simple one-step shock scenario with quick plating is similar to a single saturating pressure pulse on patch-clamp, not necessarily revealing inactivation. But the osmotic conditions in natural habitats vary. For instance, when it rains, soil bacteria at the surface would experience very different dilution kinetics from bacteria below the surface. Enteric bacteria cycling between intestines and soil live in especially complex osmotic regime. No data currently addresses the differences between abrupt and gradual shocks. Bacteria are small and are expected to swell quickly, but how the time course of tension development and decline compares to the activation, closure and inactivation kinetics of MscS in different shock regimes is unknown. All these parameters may influence survival.

To address the roles of normal MscS activation and inactivation in osmotic survival, we performed stopped-flow experiments to determine characteristic swelling and lysis times under 'instant' mixing and compared them to patch-clamp data under machine-driven tension application. We then designed parallel patch-clamp and osmotic dilution plating experiments with wild type (WT) bacteria, along with a non-inactivating mutant, G113A (*30*), and a fast inactivating mutant, D62N (*46*), and tested their viability in four

different regimes of osmotic shock.

We chose these mutants based on previous studies (*30;46;47*) suggesting at least two loci involved in inactivation. The first locus is the flexible hinge at G113 on the third transmembrane helix (TM3), shown to be involved specifically in inactivation (*30;47*). MscS' closed-to-open transition was inferred as straightening and tilting of the pore-lining TM3 helices (*30;36*), whereas the return to a non-conductive state was associated with buckling of TM3 at one of the flexible points, either G113 during inactivation or G121 during closing (*30*). Higher helical propensity in the hinge region imposed by the G113A substitution nearly abolished inactivation, thus generating a model non-inactivating mutant. The second site was D62 at the tip of the TM1-TM2 loop, which was proposed to form a salt bridge with the R128/R131 cluster on the 'cage' (*46;48*). The feasibility of the D62-R131 salt bridge formation is illustrated by a model presented in supplemental Fig. S1. Disruption of these salt bridges by D62N/R mutations leads to fast adaptation of the channel (*46*) and, as will be shown below, inactivation as well. The conformational coupling between the transmembrane and cytoplasmic 'cage' domains supporting the presence of the salt bridge was also disrupted by the D62N mutation (*49*). D62N MscS was thus chosen as a model fast inactivator. The aim of the following experiments involving these mutants is to compare the inactivation times and demonstrate the importance of inactivation in the functional cycle of MscS *in vivo*.

MATERIALS AND METHODS

Strains and mutants.

WT MscS and the mutants were expressed in MJF465 triple knockout (KO) (*mscS*$^{-}$, *mscL*$^{-}$, *mscK*$^{-}$) cells (*12*) from the pB10b vector as described previously (*16;50*). D62N originally studied in (*46*) was kindly provided by Dr. K. Yoshimura. Control MJF465 cells (KO) carried empty pB10b vector. For *in vivo* experiments, the overnight culture was diluted 1:1000 in high-osmotic medium (HiLB: 900 mOsm LB; we increased osmolarity with addition of 0.5 M NaCl) and grown for 2 hours to optical density OD_{600} of 0.4. The cells were induced at 1.5 hours with IPTG for 30 minutes, collected and then diluted into low-osmotic medium in different settings.

Stopped-flow measurements.

Cells pregrown and induced in HiLB were washed twice in Tris-buffered 900 mOsm NaCl solution (pH 7.2) and resuspended in the same buffer at OD 0.6. An Applied Photophysics SX18MV Stopped Flow machine was used to detect changes in light scattering through recording the absorbance at a wavelength of 600 nm (detection at 180 degrees, 190 V setting on PMT). The cell suspension was instantly mixed with NaCl solutions of varying osmolarity at the volume ratio of 1:10, delivered from 0.2 ml and 2 ml syringes, respectively. The light absorbance was recorded for 1 min after rapid mixing and traces from 10 consecutive trials were averaged.

Osmotic survival assays.

For single shock experiments, cells grown in HiLB were hypoosmotically downshocked in either LB/2 (200 mosm) or LB/4 (100 mosm). We made a 1:100 dilution from HiLB directly to LB/2 or LB/4 and let the bacteria adjust. The cells were further diluted (1:1000) in the respective low-osmotic medium and 150 μL was plated first at 1 minute and again at 60 minutes. Controls were diluted the same way in HiLB and plated. All plates were incubated overnight and colonies counted the following morning. All experiments represent data of at least 5 independent experiments with plating in duplicates.

For double shock experiments, cells grown in HiLB were hypoosmotically downshocked first in 700 mosm LB for 15 seconds, 1 minute, and 15 minutes, followed by a more severe downshock in either LB/2 or LB/4 for 15 minutes. Then, after reaching the identical dilution as the single shock experiments, 150 μL samples were plated on LB plates. Two controls were used in these experiments. The primary control was diluted to the same concentration in HiLB and plated. The secondary control was a 15 minute long single shock to either LB/2 or LB/4, identically diluted. As above, they were incubated overnight and the colonies counted the following morning. All percent survival calculations were done with the unshocked control taken as 100% survival.

Electrophysiology and analysis.

Giant spheroplasts were generated using the modified cephalexin method (*15;46*) with a 30 min induction by IPTG (0.8 mM). Patch clamp recordings were taken using the

same device and pipettes as outlined in Akitake, et al. (*15*). Programmed pressure protocols were delivered from an HSPC-1 pressure-clamp apparatus (ALA Instruments). All recordings were done at +30 mV in the pipette in symmetric 200 mM KCl, 90 mM $MgCl_2$ and 10 mM $CaCl_2$, 5 mM HEPES buffer (pH 7.2). After seal formation and excision, inside-out patches were subjected to 1 s linear pressure ramps and the midpoint for activation ($p_{0.5}$) was determined. We assumed that in the range of activating tensions patch curvature is constant and thus tension in the membrane (γ) depends linearly on patch radius (r) and pressure gradient (ΔP) according to Laplace's law ($\gamma = \Delta Pr/2$). For each patch individually we converted pressure into tension using the MscS tension midpoint $\gamma_{0.5}$ = 7.8 mN/m previously determined in whole-spheroplast experiments (*14*).

The thermodynamic analysis of traces was done according to two-state Boltzmann equation $Po = 1/(1+\exp((\Delta E-\gamma\Delta A)/kT)$, where ΔE and ΔA are the changes in free energy and in-plane area of the protein associated with the opening transition, *k* is the Boltzmann constant and T absolute temperature. The partial area changes between the closed (C) and open (O) conformations and the transition barrier (B) were estimated from the tension dependencies for the opening and closing rates: $\Delta A_{C\rightarrow B} = kT\cdot d\ln(k_{on})/d\gamma$ and $\Delta A_{O\rightarrow B} = kT\cdot d\ln(k_{off})/d\gamma$ (*18*).

Molecular modeling.

The D62-R131 salt bridge in MscS was first proposed in (*48*) for conformation derived from the crystal structure. The feasibility of this salt bridge for a compact resting state (*30;35*) was suggested by the molecular model presented in Fig. S1 (supplement),

along with the technical details of computation.

RESULTS

To explore the kinetics of bacterial swelling and tension onset in fast dilution experiments we measured light scattering dynamics from the bacterial suspension with the stopped flow technique. Based on this data, we chose settings for patch clamp experiments to comparably stimulate MscS over similar characteristic times in isolated membrane patches.

In the osmotic stopped-flow experiment, a small volume of dense *E. coli* suspension grown in 900 mOsm LB and equilibrated in a NaCl Tris-buffered medium of the same osmolarity was rapidly mixed with a 10x volume of lower-osmolarity buffer to obtain a final optical density between 0.07-0.05. The 10x averaged traces of the strongest shock (900→100 mOsm) are shown in **Fig. 2.1** for the three strains (WT, G113A and KO) in comparison with no shock responses.

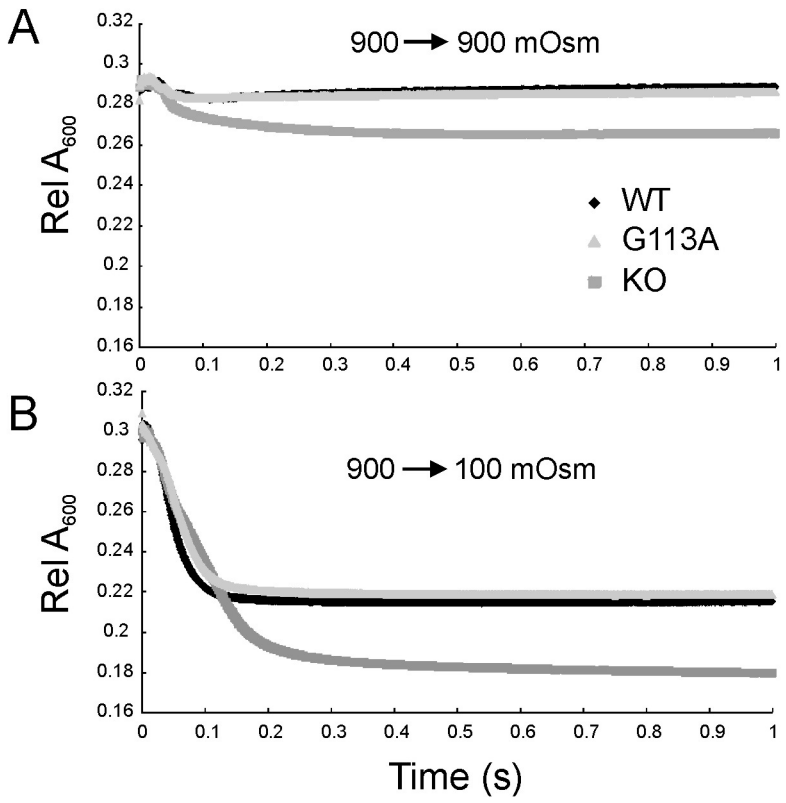

Fig. 2.1 Stopped-flow experiment with MJF 465 cells expressing WT MscS, G113A MscS or empty pB10b vector (KO). One-second traces show the dynamics of light scattering for the three cultures under no shock (900 → 100 mOsm, A) and under extreme downshock (900 →100 mOsm, B).

From absorbance kinetics one can see that unshocked control (900→900 mOsm, **Fig. 2.1A**) shows a small ~20 ms spike of optical density in WT and G113A strains, perhaps a mixing artifact or a result of cell orientation in the flow, followed by a stable absorbance in the end state. When severely shocked, (900→100 mOsm, **Fig. 2.1B**), the traces for WT and G113A show a drop of optical density within ~150 ms with a quick stabilization at a new level. The KO strain shows a deeper and slightly delayed decrease of OD with no visible stabilization of the end state within 1 s. We presume that rapidly entering a hypoosmotic solution induces cell swelling followed by osmolyte release. Swelling increases cell size, which can increase scattering, but at the same time swelling

dilutes the cytoplasm, thus decreasing refractive index and scattering. In cells containing WT MscS, we expect MscS to respond to swelling with a rapid osmolyte efflux, whereas in the unprotected KO cells, which lack MscS and two other MS channels, severe osmotic downshock was expected to cause osmolyte efflux through non-specific membrane cracks and lethal damage (*12*).

As seen from Fig. 2.1B, the traces for WT and the G113A non-inactivating mutant essentially coincide, quickly stabilizing at a new level. The WT's ability to inactivate does not produce any substantial difference in optical responses compared to the non-inactivating G113A, suggesting the massive release of osmolytes occurring in this time scale does not involve inactivation. The stabilization of absorbance after the initial drop likely represents channel closure upon pressure release. The fast-inactivating D62N mutant exhibited a partial loss-of-function phenotype compromising viability at these shocks (*46*), for this reason it was not included in these trials. In the following experiments we compared the responses of WT MscS-expressing bacteria with the KO strain devoid of three major MS channels.

Four trials with a progressively increasing amplitude of shock (**Fig. 2.2**) show decreasing optical density due to decreased scattering.

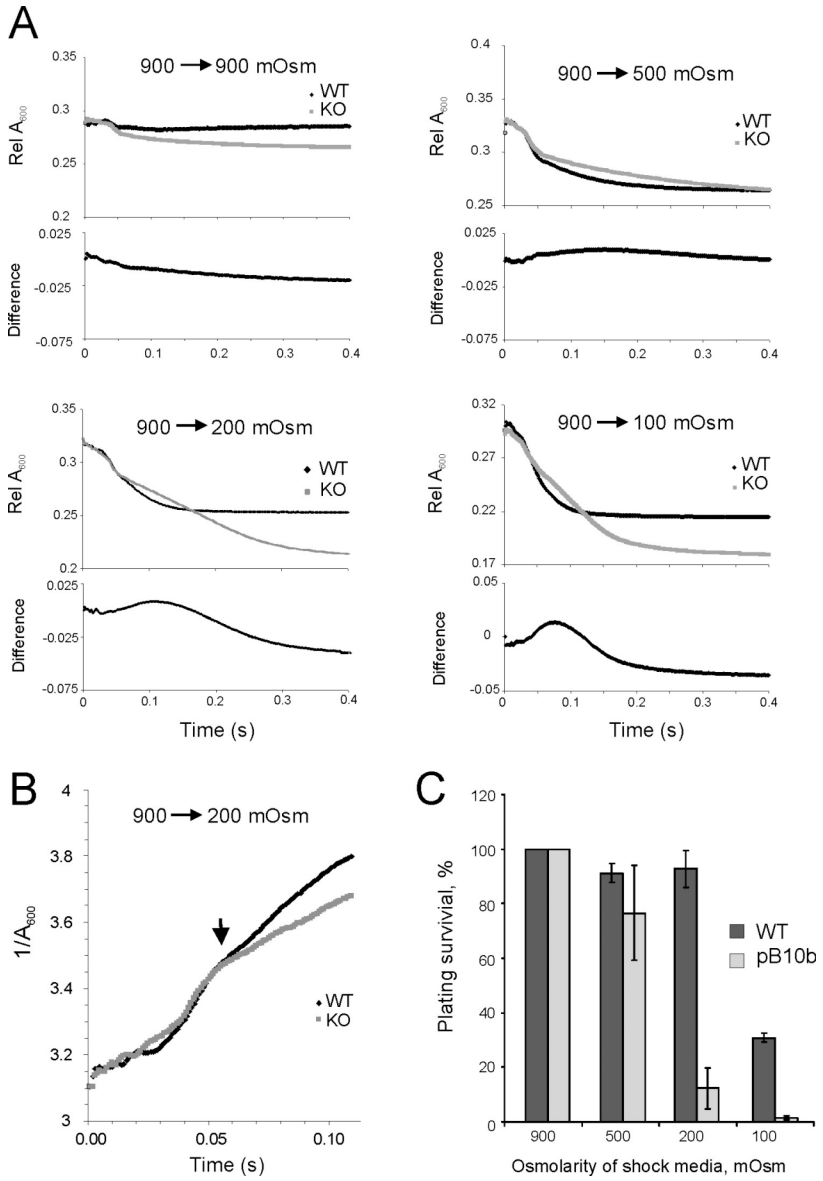

Fig. 2.2. Bacterial swelling response in a stopped flow apparatus correlates with osmotic survival. The smaller syringe contained a dense suspension of *E. coli* cells pre-adapted at 900 mOsm, and the larger syringe contained buffers of varying osmolarity. (A) Absorbance (A_{600}) traces from MscS WT and from empty vector control (KO) injected at the same density. Data shows a time-dependent decrease of scattering (top panels). Lower traces in each set represent the difference between WT and KO responses. Under strong shocks (900 → 200 and 900 → 100 mOsm), KO cells loose viability and the difference peak reflects osmotic damage following swelling. (B) Inverse absorbance (A^{-1}) in the 900 → 200 mOsm as a function of time, the arrow shows the 50 ms time point at which the traces deviate marking the onset of permeability. (C) Osmotic survival of *E. coli* cells under similar shock conditions as determined with plate counts. Plating was done 10 min after dilution. Error bars represent standard deviation (n=5).

Under no shock conditions, the KO cells reproducibly featured a slow decrease of optical density and, as a result, the difference trace (KO minus WT, bottom of each panel) shows a gradual decrease. The 900→500 mOsm dilution shows a biphasic response in both WT and KO cells, with a fast scattering drop that similarly completes within ~50 ms and a slower phase that is slightly delayed in KO; the difference trace bulges up with a shallow maximum near 150 ms. Shocking from 900 to 200 mOsm produces a considerably deeper but slower drop of scattering for KO with a more pronounced difference peak near 100 ms. The final most extreme 900→100 mOsm shock produces a similar response with a delayed 'shoulder' in KO cells, which produces a sharper difference peak.

Cell survival determined under shocks of the same magnitude (**Fig. 2.2C**) shows KO viability drops precipitously under a 900 to 200 mOsm downshock, whereas cells expressing WT MscS survive and experience significant viability loss only when downshocked from 900 to 100 mOsm. The first notch in the light scattering data in both cultures' responses may reflect mixing/shearing events, while the short plateau and the beginning of scattering drop represent the period of cell swelling (dilution of internal content) when pressure/tension are building up. Fig 2B represents the beginning of the same response plotted as the inverse absorbance (A^{-1}) known to be linearly related to the cell volume ($dV/dt=k(dA^{-1})/dt$, where k is a constant (*51*)). The empirical relationships between absorbance and volume had been worked out for lipid vesicles (*51*) and mitochondria (*52*) which behave largely as ideal osmometers. Since *E. coli* cells are surrounded by elastic cell wall (*53*), we do not expect them to behave as osmometers, and thus direct calibration of the scattering response against equilibrium cell volume is

difficult. In the course of the first 50 ms, A^{-1} in both WT and KO cultures increases concomitantly by ~10% reflecting swelling (**Fig. 2.2B**), but after that point (arrow) the traces deviate. WT's further fast scattering drop likely reflects osmolyte efflux through activated channels, which stops when pressure is partially relived and channels close. The deeper, slower and continuing scattering drop in KO likely indicates leaks through membrane tears, which do not reseal in the time course of 0.4 s (no plateau). The deeper drop of scattering in KO likely indicates more swelling and/or continuing loss of intracellular constituents. The difference peak on each panel is roughly proportional to the difference in the fraction of dead cells (**Fig. 2.2C**) and may reflect the time course of irreversible osmotic damage. From the traces we conclude that the time of swelling/pressure buildup can be estimated as 30-50 ms, whereas the time of non-lethal equilibration (in WT) shortens with the shock amplitude and reaches completion between 100 and 300 ms.

Thus, MscS should respond rapidly to the 30 ms pressure buildup, and the slope of channel activation rate as a function of tension would determine the response speed. Another question is how quickly the channel will close if tension drops from a super-threshold level to some intermediate sub-threshold level following osmolyte release. We have attempted directly assessing MscS' opening and closing rates under step pressure protocols delivered from a pressure clamp apparatus. **Fig. 2.3A** shows a series of patch current responses to 0.2 s long pressure steps of increasing amplitude.

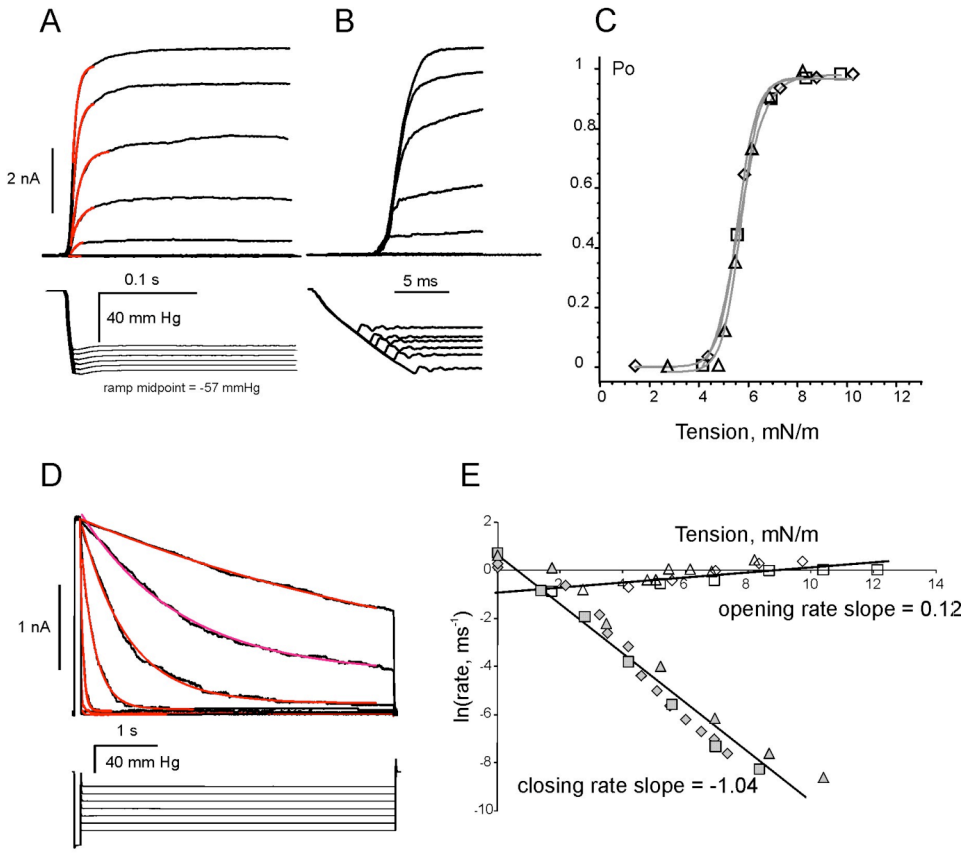

Fig. 2.3. Tension dependencies of MscS opening and closing. (A) Kinetics of MscS opening in response to a series of pressure steps (10 ms raise time). (B) Expanded initial region of the traces in (A) illustrating current onset. (C) The dose-response curve (Po(γ)) obtained from the steady-state current levels in (A) fitted with Boltzmann equation that predicts the energy gap between the states $\Delta E = 14.5$ kT, and the in-plane protein expansion $\Delta A = 10.5$ nm^2. (D) Kinetics of MscS closure at different pressures after opening by a short saturating pulse. (E) Tension dependencies of the opening and closing rate constants obtained from monoexponential fits of traces in (A) and (B) shown in red. The opening (open symbols) and closing (filled symbols) rates are shown for three independent patches and fitted together. The slope of the apparent opening rate suggests $\Delta A_{C\rightarrow B} = 0.5$ nm^2 in-plane expansion between the closed-state well and rate-limiting barrier and the closing rate dependency predicts $\Delta A_{O\rightarrow B} = 4.3$ nm^2 for the area change from the open well to the barrier. Note that the sum of $\Delta A_{C\rightarrow B}$ and $\Delta A_{O\rightarrow B}$ is less than total ΔA predicted by the Boltzmann fit of the instantaneous dose-response curve (C).

The red color indicates the segments of traces fitted with monoexponential functions, approximating opening rates. The expanded current and pressure stimulus traces (**Fig. 2.3B**) indicate that the machine-limited pressure onset is not instantaneous, but rather is a nearly linear ramp with the slope of ~5 mm Hg/ms. The threshold of about 45 mm Hg for that particular patch is reached within 8 ms, and the first super-threshold step activates

~15% of channel population within 2 ms. Further pressure buildup increases the fraction of active channels and the current grows concomitantly with pressure, but each time the current quickly levels off. The exponential fits in **Fig. 2.3A** show that the apparent initial rate is in the order of ms^{-1} which increases shallowly with increasing pressure (**Fig. 2.3E**). The onset of pressure stimulus is obviously not fast enough to resolve the first-order kinetics of MscS as the current closely follows the changing pressure stimulus. The slow onset of pressure may thus underestimate the intrinsic rate of MscS opening, which appears to be faster than indicated in **Fig. 2.3E**. Yet, the experiment shows that MscS is able to respond quickly to 10-15 ms ramps of pressure and reach 90% of activity within 5 ms, beating cell swelling. The fast response to sub-lytic tension ensures that the 'valve' will open and release before the intracellular pressure reaches lytic limit in the event of abrupt dilution.

Using the steady-state levels obtained at different tensions (**Fig. 2.3A**) we created a dose-response curves, represented in **Fig. 2.3C**. Fitting this curve with the two-state Boltzmann equation (see legend) estimated the energy gap between the open and closed states (ΔE) as 14.5±0.8 kT and the in-plane area change (ΔA) as 10.5±0.5 nm^2 (n=3) consistent with previous results (*14;15*).

Fig. 2.3D shows the closing kinetics recorded with a two-pulse protocol. The first short saturating pulse opens the entire population (~100 channels) in the excised patch, whereas the following longer step of variable amplitude conditions the closing process. Closing of MscS is slower than opening and is well resolved. From the exponential fits of the decaying currents (red lines, panel D) we determined the closing rate dependency on tension (**Fig. 2.3E**). The slope predicts that the conformation representing the rate-

limiting barrier for closing has approximately 4.3 nm^2 smaller footprint in the plane of the membrane than the open conformation ($\Delta A_{O\rightarrow B}$). Given that the total in-plane expansion (ΔA) of the protein is ~10.5 nm^2, this distance predicts that the rate-limiting barrier is positioned roughly two thirds of the expansion trajectory toward the open state. Note that the tension dependency of the opening rate was not adequately measured with the available pressure protocol and thus the deduced area change from the closed well to the rate-limiting barrier ($\Delta A_{C\rightarrow B}$ = 0.5 nm^2) is severely underestimated (**Fig. 2.3E** and legend). Even in the simplifying assumption of single-barrier transition in MscS (*54*), we do not expect that the sum of $\Delta A_{C\rightarrow B}$ and $\Delta A_{O\rightarrow B}$ should correspond to the total ΔA predicted by the Boltzmann fit of the instantaneous dose-response curve (**Fig. 2.3C**).

The tension dependency of the closing rate (**Fig. 2.3E**) permits a rough estimation of the residual tension in the cell membrane after the shock. If we take 200 ms as a characteristic time for the osmotic equilibration process completion, then, after activating at 8-10 mN/m, the tension may drop to the residual level of 3-3.5 mN/m to assure the closing process with this characteristic time. Tension in the membrane does not have to drop to zero, it should simply be 1-2 dynes below the threshold of ~5 mN/m (**Fig. 2.3C**).

Next we addressed the time course and nature of MscS inactivation, which is normally a slow tension-driven process (*15*). The physiological meaning of MscS inactivation has not been addressed, and we hypothesize it might be important for cell survival under mild or gradually imposed shocks. The two-syringe stopped-flow technique, however, does not permit us to observe the light scattering changes that would happen in the event of slow or multi-step dilution. By comparing inactivation kinetics in WT and mutants with both fast- and noninactivating phenotypes on patch clamp and *in*

vivo shock experiments, we evaluated whether WT's slow adaptive behavior confers a survival advantage.

As mentioned in the introduction, we took cues from the models shown in Fig. S1 to choose the mutants for our studies. Previously, the D62-R131 salt bridges were predicted from functional studies (*46;49*) but were not present in either the crystal structure (*1;31*) or in the compact models of the resting state (*34;35*). The model derived using EMP confirms the possibility of salt-bridge formation, in which likely stabilizes TM2-TM3 interactions providing a mechanical link between the lipid-facing helices and the gate (*37*). This conformation is also predicted to stabilize the absence of G113 kinks in the resting state. Disruption of the salt bridges by the D62N substitution possibly destabilizes the TM2-TM3 association and increases the probability of G113 kink formation leading to inactivation. Higher helical propensity in the G113A mutation, on the other hand, precludes inactivation (*30*).

Fig. 2.4 shows patch-clamp traces recorded from the fast inactivating mutant D62N, WT, and the noninactivating mutant G113A responding to both saturating ramps of varying duration and a prolonged subsaturating pressure step followed by a saturating pulse.

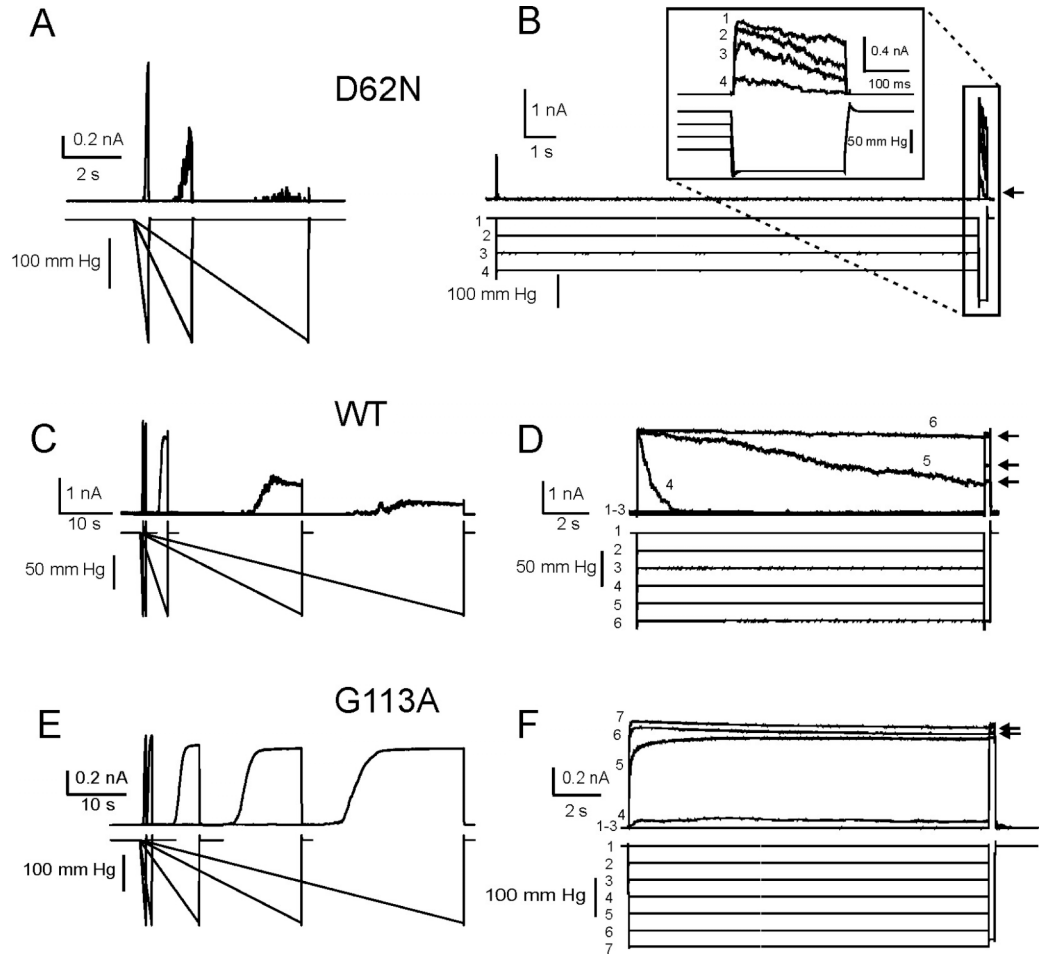

Fig. 2.4 Inactivation of WT MscS and the D62N and G113A mutants as observed by two protocols. The first protocol (panels A, C, E) involved saturating ramps of various durations. The second protocol (B, D, F) was a 15 s pre-conditioning step followed by a short saturating pulse revealing the non-inactivated fraction of the channel population. D62N shows increased inactivation relative to WT in ramp experiments (A), and a silent inactivation bypassing the open state under pulse stimuli (B). G113A shows virtually no inactivation (E, F).

From the saturating ramp data, we see the entire channel population on a patch responds to a short ramp, evident from the high conductance level. As the ramps become progressively longer, the maximal current achieved diminishes in both the fast inactivating D62N as well as WT (panels A and C). For example, WT shows only 15% of maximum conductance with a 60 s ramp, so approximately 85% of the WT channel population is inactivated. The other protocol, the 15-second pressure step, shows the inactivated MscS fraction depends not only on speed of onset of pressure stimuli, but also

on sustained sub-saturating pressure (**Fig. 2.4B, D, F**). While current can decline as a result of reversible adaptation (*14;30*), we differentiate between nonconducting responsive (adapted) channels and nonconducting inactivated channels with a short saturating test pulse at the end of the 15 s step. Inactivated channels do not respond. Maximal inactivation was observed at higher pressures still permitting adaptive closure since normally MscS inactivates from the closed state when subjected to tension (*44*), and inactivation onset essentially coincides with the activation threshold. Overall, a 15 s constant-pressure stimulation thus is capable of driving about 50% of the WT population to the inactivated state (**Fig. 2.4D**). Traces obtained with similar protocols for G113A show less than 10% inactivation during 15-60 s stimulation. In the case of the fast-inactivating D62N, 90% of the channels inactivate with a 5 s saturating ramp, which is an order of magnitude faster than WT. D62N also exhibits silent inactivation, which is inactivation under sub-threshold tensions bypassing the open state. Only the highest amplitude step (**Fig. 2.4B**) invokes a brief transient response, but the test pulse in the end reveals that ~80% of the population is inactivated. Based upon these observations, we conclude that D62N MscS inactivates much faster when conditioning tension approaches or exceeds the activating threshold.

To reveal the differences in cell survival caused by different inactivation time courses, in the first experiment, we subjected all three strains to intense 'short' (1 min) and 'long' (60 min) osmotic shocks (Fig. 5A) followed by plating on regular LB plates. With a downshift from 900 to 100 mOsm, WT and G113A survived comparably 1 min shock (~80%), but the longer exposure resulted in a lower survival of G113A. D62N was previously reported to have a higher activation threshold and partial loss-of-function

phenotype (*46*), and hence its survival in the same shock medium was too low to draw meaningful conclusions about its behavior. For this reason, it was only shocked from 900 to 200 mOsm. The survival of this mutant did not decline with the time of exposure to low osmolarity (Fig. 5A, right panel).

The second, two-step protocol was designed to mimic gradual osmolarity downshift (Fig. 5B). Bacteria pre-equilibrated at 900 mOsm were first subjected to a 900→700 mOsm pre-shock and then, after a varied period at intermediate osmolarity (Δt), they were further diluted down to 200 mOsm. The survival of WT and G113A was not substantially compromised by the exposure to the intermediate osmolarity, but the fast inactivator showed a minimum of survival at Δt=0.25 min (15 s). The data suggests the inactivating mild pre-shock increases fatalities from the final shock and it affects D62N significantly more than both WT and G113A.

DISCUSSION

Based on the small size and large surface area-to-volume ratio, it was always assumed that osmotic swelling of bacteria should be faster than a second, but characteristic time measurements can hardly be found in the literature. Previously, stopped-flow was used to study solute transport processes in bacteria (*55;56*) but not fast osmotic swelling. Here we presented light scattering responses of high-osmolarity adapted *E. coli* populations upon rapid (~3 ms) mixing with a hypotonic medium. How a cell suspension scatters light depends on the size, shape and refractive index of the cells (*57*). Consistent with previously reported data for mitochondria (*52*) and vesicles (*51*), the major effect of hypoosmotic shock is decreased scattering. This is largely a result of

cytoplasmic dilution due to swelling and subsequent osmolyte efflux. When rod-shaped bacteria delineated by an elastic cell wall swell, we believe there is no dramatic dimensional change. Instead, they may become slightly rounded. When shocked, light scattering time courses for the MscS-expressing and control knock-out (KO) cells initially coincide (**Fig. 2.2A,B**). This suggests that the first 30-50 ms stage where scattering drops by 7-10% reflects cell swelling, which does not involve MscS activation. The subsequent deviation of traces – apparent in the steeper scattering decrease in MscS-expressing cells – likely reflects rapid ion and small osmolyte efflux through activated channels. It signifies that swelling at this time generates super-threshold tension, and the high slope of signal change likely reflects the maximal open probability. The optical response of MscS-expressing cells plateaus in 100-150 ms, which may indicate that either tension is now below the threshold and the channels are closed, or the pool of permeable osmolytes is exhausted and the cell size and refractive index do not change any more. Without detailed calibration of the optical response of cell suspensions (*51;52*) we were unable to determine absolute values of volume change prior to the permeability onset and the presented information is limited to the time domain. The coincidence of traces obtained with WT and G113A MscS (**Fig. 2.1**) suggests that inactivation does not contribute to the optical response reflecting efflux kinetics at this time scale.

In the absence of channels (KO cells) the light scattering response is longer and of larger amplitude (**Fig. 2.1** and **2.2**). Two different phases are apparent, an initial shorter phase and a second longer one. As stated above, the first phase (0-50 ms) is similar in both WT and KO and likely represents initial swelling. The second longer stage in the KO strain most likely corresponds to excessive swelling and loss of membrane integrity.

The scattering eventually reaches a lower level possibly due to more cytoplasmic depletion through a different pathway, likely non-specific membrane 'cracks.' The slower scattering change suggests the overall permeability of the cracks is lower than that of the channel population. It is also possible that the rate of crack formation is slower than the opening rate of MscS, and this needs to be further quantified. The cracks also do not reseal since the scattering keeps changing throughout the entire 1 s observation period (**Fig. 2.1**). A dramatic cell viability drop assayed under similar shock conditions (**Fig. 2.2C**) indicates massive damage, which correlates with the amplitude of the 'hump' in the difference traces (**Fig. 2.2A**). Under 900→200 and 900→100 mOsm down-shifts, only 14% and 2% of KO cells survive, whereas WT MscS rescues 95% and ~30% of cells, respectively, through MscS activation lasting ~50-100 ms based on the scattering responses.

The patch-clamp data collected on WT MscS (**Fig. 2.3**) shows the channel population readily opens to machine-generated (10-15 ms raise time) pressure steps, and saturation is reached at ~8 mN/m (**Fig. 2.3C**), substantially below lytic tensions of 12-15 mN/m, at which the large-conductance MscL channel activates (*14;18*). After reaching the tension threshold of ~5 mN/m (Fig.3A-C), MscS population activates with a characteristic time of 1-3 ms, and the active fraction steeply grows with tension. Although the machine-limited pressure onset speed was too slow to determine the first-order rates of MscS activation, the data illustrates that the channel activity follows the tension increase with a minimal delay. The full response developing between 5-7 mN/m within 3 ms (**Fig. 2.3B,E**) shows that MscS easily 'keeps up' with the pressure build up in the swelling bacterial cell and opens well before tension reaches lytic limit. The recently

published fitting of MscS ramp responses with QuB suggested that the opening rate grows exponentially 12.7 times per 1 mN/m of tension increase (*54*). This should provide the basis for estimation of the MscS opening latency at super-threshold tensions. The characteristic time of the MscS opening process itself has been estimated in high time resolution patch-clamp experiments to be shorter than 3 μs (*58*).

When some cytoplasmic osmolytes are released and tension in the membrane drops, the channels close. We can confidently resolve the closing rate dependence on tension. When extrapolated to zero, it predicts that MscS can close within a millisecond. At 3 mN/m the population relaxes from the fully open to the closed state with a characteristic time of ~60 ms (**Fig. 2.3D,E**). The scattering traces from WT-MscS (**Fig. 2.2**) level off within ~50 ms of channel activation, which suggests that if a residual tension in the bacterial membrane persists after the shock, then it should be below 3 mN/m. Thus, comparing observed characteristic times from light-scattering and patch-clamp data gives us a range for membrane tension development in intact cells during osmotic shock *in vivo*.

As illustrated in **fig. 2.4**, MscS inactivation is a slow process. The channel does not respond to even super-saturating tension in the inactivated state (*15*). It has been previously hypothesized that inactivation prevents cellular 'bleeding' under prolonged exposure to hypotonic medium when tension may be near the activation threshold. Previous studies produced non-inactivating and fast-inactivating (*30;46*) mutants which helped us address the biological role of inactivation and its slow kinetics. Ramps and steps were used to characterize the rate of inactivation (**Fig. 2.4**). WT MscS readily responds to an abrupt tension onset, but most of the channels inactivate under 30-60 s

ramps. For the fast-inactivating D62N mutant, it takes only a five-second ramp to inactivate nearly the entire population, whereas G113A shows little inactivation under a 60 s ramp.

Single-step shocks performed with these mutants (**Fig. 2.5A**) have indicated the viability of D62N is generally compromised compared to WT and G113A but is essentially independent of the length of exposure to the hypotonic medium.

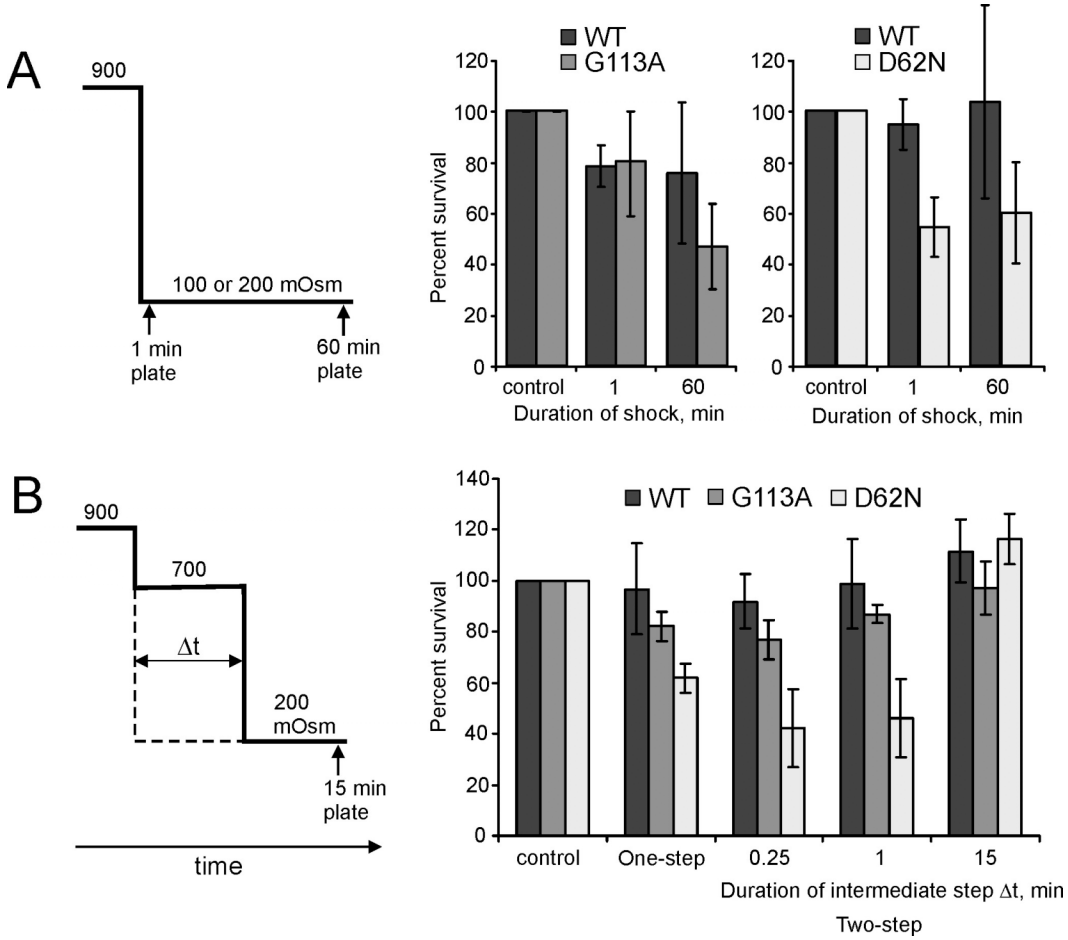

Fig. 2.5. The survival of *E. coli* MJF465 cells expressing WT MscS, non-inactivating G113A or fast-inactivating D62N mutants in different regimes of osmotic shock. (A) The dependence of WT and G113A survival on the duration of exposure to low-osmotic medium (1 or 60 min) after the 900→100 mOsm shock. The values for WT (79±24%) versus G113A (47±19%) at 1 min are statistically indistinguishable (n=6), whereas at 60 min the values were different with a t-test value of 0.07. The viabilities for G113A at 1 min (82±22%) and 60 min were different with a t-test value of 0.02. D62N was shocked into 200 mOsm along with WT controls. The survivals after 1 and 60 min for both strains were the same. (B) The average percent survival of WT, G113A, and D62N when subjected to a 15 minute single shock and double shocks of varying duration. D62N has the lowest survival under the two-step shock regime. The error bars

represent standard deviations (n=6). The D62N data for the 0.25 and 1 min double shocks are different from one-step shock data with a t-test value of 0.09.

G113A survived long (60 min) shocks less than short shocks (1 min), which confirms inactivation assists recovery during or after the shock. The two-step shock protocol revealed the fast-inactivating mutant's vulnerability when mildly pre-shocked for a short period of time (15-60 s), which apparently drives most of the channel population to the inactivated state prior to stronger second shock. Importantly, extending the pre-shock time to 15 min restores D62N's ability survive likely because the cells adapted to the medium shock and the channels recovered. The above experiments illustrate why WT MscS inactivation is present yet slow. Indeed, after an abrupt down-shock and initial osmolyte release (when there is no real danger of membrane rupture), while the cell remains in a moderately hypotonic medium, the non-inactivated MscS might be flickering and disrupting vital gradients. Inactivation is highly beneficial for recovery. On the other hand, if inactivation is too fast, it may dangerously turn off the channel population during a gradual osmotic shock (such as in gentle rain), denying protection when conditions worsen.

In conclusion, the comparison of *in vivo* responses with characteristic MscS activation and closure times illustrate that abrupt shock fully activates MscS before pressure reaches lytic levels, followed by prompt closure upon partial osmotic equilibration of the cell. Under prolonged shocks, gradual inactivation prevents continuous channel activity and assists recovery. Based upon *in vivo* assays conducted in the absence of MscL, inactivation appears to be a vital part of MscS' functional cycle and

not a patch clamp artifact.

Acknowledgement

The work was partially supported by NIH grant GM075225 to SS. The authors thank Dr. Ian Booth for the MJF465 strain and Dr. George Lorimer and Sarah Wehri for assistance with stopped flow experiments. The authors also thank Mrs. Naili Liu for general laboratory assistance and Dr. Kenjiro Yoshimura for the D62N mutant and helpful discussions.

Supporting Information

The steric feasibility of the D62-R131 salt bridged conformation is illustrated in Supplemental Figure S1 along with the technical details of the modeling process and a brief discussion of functional implications for the stability of the resting state (http://pubs.acs.org/journal/bichaw).

Chapter 3

Conclusion

The experiments discussed in this document were undertaken with the ultimate goal of increasing our understanding of how MscS functions. My research examined MscS with live-cell techniques, plating and light scattering, so the channel could be assessed *in vivo*. The plating experiments demonstrated that inactivation is not just a patch clamp artifact; it does in fact optimize MscS activity to maximize bacterial survival in different hypoosmotic shock situations. Additionally, the light scattering data showed us the difference in changing refractive indices between hypoosmotically shocked *E. coli* with and without MscS. Overall, the experiments successfully probed the hypotheses they were designed to explore.

We can say that inactivation is an important part of MscS function *in vivo*, and we can see how the channel's presence aids hypoosmotically shocked cell survival via plating and light scattering, respectively. In the future, it may be beneficial to apply the light scattering technique to mutants with known impaired opening phenotypes. There are several, which have been explored but are not discussed in this document; they are N167V, F151A, N167D, and G168E. The reasons for choosing specifically those four mutants are the following: N167V opens extremely reluctantly even when pulsed, and in contrast, G168E opens very easily and remains in that state compared to WT. F151A and N167D both lack hysteresis. A lack of hysteresis means that as negative pressure is applied in a ramp, a certain number of channels open at a given tension, and as tension is released, we see the same channel response. WT does show moderate hysteresis, meaning that as tension is released, we do not see the same channel response. F151A's

activation midpoint is not shifted from WT, whereas N167D opens at near-lytic tensions with MscL. From light scattering, we see a clear difference with MscS present and without, and this may be a powerful technique that could allow us to observe the following:

- Can we see the effect(s) of no hysteresis (F151A, N167D) during hypoosmotic shock relative to WT, and does a shifted activation midpoint impact cellular response in two non-hysteretic mutants?
- Does a channel with exaggerated hysteresis (G168E) remain open in a cell the same way as it does on patch clamp?
- Will a channel that is extremely unstable in the open state on patch clamp (N167V) show a smaller change in refractive index, or is the channel response so dampened that it looks like the KO *in vivo*?

In terms of quantitative analysis, light scattering provides values for changes in absorbance as a function of time; both values can be assessed for each mutant to determine the effects of perturbed opening kinetics on MscS function *in vivo*.

Along with continuing light scattering experiments, it would be prudent to explore whether MscS has more stable conformations than just closed, open, and inactive. There are two basic observations that imply MscS is not a three state channel. First, the presence of hysteresis in WT and our ability to remove it while not adversely affecting its activation midpoint as observed in the F151A mutant tells us that there is more than one open state. Additionally, the single monoexponential decay used to approximate WT's closing rate has proven to be insufficient for nearly all the mutants mentioned above, a second observation telling us that MscS has more than three states. It would certainly be

a worthwhile endeavor to take closing traces of the beta domain mutants like those of WT and fit them in a program like QuB to obtain multiple rate constants.

Appendix A

Supplemental Figure

Adaptive MscS gating in the osmotic permeability response in *E. coli*: the question of time

Miriam Boer, Andriy Anishkin and Sergei Sukharev*

Department of Biology, University of Maryland, College Park, MD 20742

Reconstruction of the complex functional cycle of MscS from the single crystal structure requires extensive modeling and inputs from experimental analysis (*35*). The possibility of the D62-R128 salt bridge formation between the tip of the TM1-TM2 loop (D62) and the upper hemisphere of the cytoplasmic 'cage' domain (R128, R131) was first noticed by Sotomayor and Schulten in MD simulations of MscS original crystal structure (*59*), but in none of the following models of the resting (*34;35*) or open (*33;36*) states the D62-R128 or D62-R131 bridges were present. The bridges are not present in the crystal structure of A106V MscS either, which likely represents a conductive state. Only the subsequent functional analysis of these sites by Yoshimura and coworkers (*46*) demonstrated that mutations disrupting putative salt-bridges (D62N, R) strongly destabilize the open state increasing the rate of adaptive closure and lead to partial loss-of-function phenotypes, whereas the swapping of charges by the double D62R/R131D mutation restores the WT-like phenotype. We have attempted visualization of the salt-bridged conformation through modeling.

Molecular modeling.

The model was created from the crystal structure of MscS (PDB ID 2OAU) (*60*) with a reconstructed N-terminal domain (Fig. S1A) using the extrapolated motion protocol (EMP) (*35;36*) consisting of the recursive cycles of small structural displacements, energy minimizations and short relaxing MD simulations. This protocol propagates protein motion in smooth trajectories and generally preserves the secondary structure of the protein. Multiple EMP trials of full MscS generated ~55000 different conformations which were sorted using a special VMD script for detection of structures satisfying a set of constraints: formed D62-R131 bridges, tight TM2-TM3 contact, compact TM3 barrel with a closed gate. The structure scored the highest was selected as the current model of the resting conformation (Fig. S1B).

In contrast to the splayed positions of the TM1-TM2 pairs in the crystal structure, the model features reconstructed TM2-TM3 contacts (*35*) shown to be necessary for proper transmission of stress from the lipid bilayer to the gate located within the pore (*37*). It appears that the TM2-TM3 association is strongly stabilized by the D62-R131 salt bridges connecting the TM1-TM2 loops with the cytoplasmic 'cage' domain. Disruption of these salt bridges by D62N/R mutations leads to fast adaptation and inactivation of the channel (*46*). D62N MscS was thus chosen as a model fast inactivator.

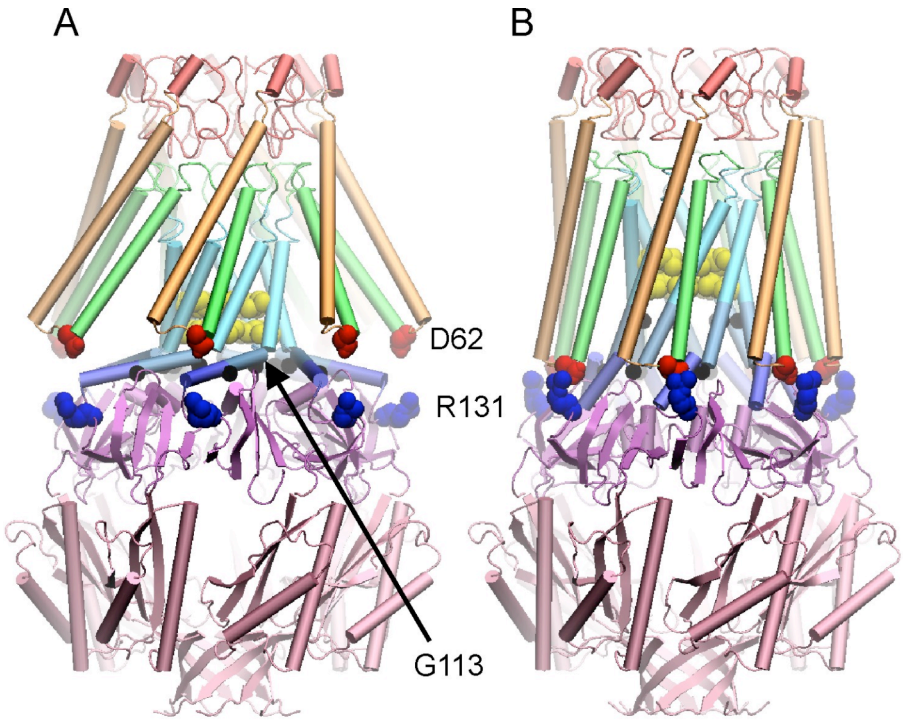

Fig. S1. Positions of mutations leading to slow- and fast-inactivating phenotypes. The model of MscS directly derived from the crystal structure (PDB ID 2OAU) by attaching N-terminal domains (A) and the model of the resting state with repacked peripheral TM1 (gold) and TM2 (green) helices (B) stabilized by D62-R131 salt bridges. In the crystal structure D62 (red) on TM1-TM2 loops are separated by ~7Å from R131 (blue) on the cytoplasmic 'cage' domain. The crystal structure also shows a vivid G113 kink attributed to the inactivated state (*61*). The structures illustrate the putative roles of the D62N mutation that leads to fast inactivation through separation of TM2 from TM3 and the G113A mutation that decreases the likelihood of the G113 kink formation leading to a slow-inactivating phenotype. The hydrophobic gate formed by the rings of L105 and L109 is shown as yellow spheres.

References

1. Bass, R. B., Strop, P., Barclay, M., and Rees, D. C. (2002) Crystal structure of Escherichia coli MscS, a voltage-modulated and mechanosensitive channel, *Science (New York, N. Y 298*, 1582-1587.

2. Chang, G., Spencer, R. H., Lee, A. T., Barclay, M. T., and Rees, D. C. (1998) Structure of the MscL homolog from Mycobacterium tuberculosis: a gated mechanosensitive ion channel, *Science 282*, 2220-2226.

3. Sachs, F. (1992) Stretch-sensitive ion channels: an update, *Soc. Gen. Physiol Ser. 47*, 241-260.

4. Sukharev, S. and Corey, D. P. (2004) Mechanosensitive channels: multiplicity of families and gating paradigms, *Sci. STKE. 2004*, re4.

5. Hamill, O. P. and Martinac, B. (2001) Molecular basis of mechanotransduction in living cells, *Physiol Rev. 81*, 685-740.

6. Guharay, F. and Sachs, F. (1984) Stretch-activated single ion channel currents in tissue-cultured embryonic chick skeletal muscle, *J. Physiol 352*, 685-701.

7. Zhou, X. L., Loukin, S. H., Coria, R., Kung, C., and Saimi, Y. (2005) Heterologously expressed fungal transient receptor potential channels retain mechanosensitivity in vitro and osmotic response in vivo, *Eur. Biophys J 34*, 413-422.

8. Vriens, J., Watanabe, H., Janssens, A., Droogmans, G., Voets, T., and Nilius, B. (2004) Cell swelling, heat, and chemical agonists use distinct pathways for the activation of the cation channel TRPV4, *Proc. Natl. Acad. Sci. U. S. A 101*, 396-401.

9. Patel, A. J. and Honore, E. (2001) Properties and modulation of mammalian 2P domain K+ channels, *Trends Neurosci. 24*, 339-346.

10. Coste B, et al. (2010) Piezo1 and Piezo2 Are Essential Components of Distinct Mechanically Activated Cation Channels, *Science 330*, 55-60.

11. Sukharev, S. I., Blount, P., Martinac, B., Blattner, F. R., and Kung, C. (1994) A large-conductance mechanosensitive channel in E. coli encoded by mscL alone, *Nature 368*, 265-268.

12. Levina, N., Totemeyer, S., Stokes, N. R., Louis, P., Jones, M. A., and Booth, I. R. (1999) Protection of Escherichia coli cells against extreme turgor by activation of MscS and MscL mechanosensitive channels: identification of genes required for MscS activity, *The EMBO journal 18*, 1730-1737.

13. Chiang, C. S., Anishkin, A., and Sukharev, S. (2004) Gating of the large mechanosensitive channel in situ: estimation of the spatial scale of the transition from channel population responses, *Biophys. J. 86*, 2846-2861.

14. Belyy, V., Kamaraju, K., Akitake, B., Anishkin, A., and Sukharev, S. (2010) Adaptive behavior of bacterial mechanosensitive channels is coupled to membrane mechanics, *J Gen Physiol 135*, 641-652.

15. Akitake, B., Anishkin, A., and Sukharev, S. (2005) The "dashpot" mechanism of stretch-dependent gating in MscS, *The Journal of general physiology 125*, 143-154.

16. Sukharev, S. (2002) Purification of the small mechanosensitive channel of Escherichia coli (MscS): the subunit structure, conduction, and gating characteristics in liposomes, *Biophysical journal 83*, 290-298.

17. Moe, P. and Blount, P. (2005) Assessment of Potential Stimuli for Mechano-Dependent Gating of MscL: Effects of Pressure, Tension, and Lipid Headgroups, *Biochemistry 44*, 12239-12244.

18. Sukharev, S. I., Sigurdson, W. J., Kung, C., and Sachs, F. (1999) Energetic and spatial parameters for gating of the bacterial large conductance mechanosensitive channel, MscL, *J. Gen. Physiol 113*, 525-540.

19. Martinac, B., Buechner, M., Delcour, A. H., Adler, J., and Kung, C. (1987) Pressure-sensitive ion channel in Escherichia coli, *Proceedings of the National Academy of Sciences of the United States of America 84*, 2297-2301.

20. Sukharev, S. and Anishkin, A. (2004) Mechanosensitive channels: what can we learn from 'simple' model systems?, *Trends Neurosci. 27*, 345-351.

21. Epstein, W. (2003) The roles and regulation of potassium in bacteria, *Prog. Nucleic Acid Res. Mol. Biol. 75*, 293-320.

22. Wood, J. M., Bremer, E., Csonka, L. N., Kraemer, R., Poolman, B., van der, H. T., and Smith, L. T. (2001) Osmosensing and osmoregulatory compatible solute accumulation by bacteria, *Comp Biochem. Physiol A Mol. Integr. Physiol 130*, 437-460.

23. Schumann, U., Edwards, M. D., Rasmussen, T., Bartlett, W., van, W. P., and Booth, I. R. (2010) YbdG in Escherichia coli is a threshold-setting mechanosensitive channel with MscM activity, *Proc. Natl. Acad. Sci. U. S A 107*, 12664-12669.

24. Li, Y., Moe, P. C., Chandrasekaran, S., Booth, I. R., and Blount, P. (2002) Ionic regulation of MscK, a mechanosensitive channel from Escherichia coli, *EMBO J. 21*, 5323-5330.

25. Berrier, C., Besnard, M., Ajouz, B., Coulombe, A., and Ghazi, A. (1996) Multiple mechanosensitive ion channels from Escherichia coli, activated at different thresholds of applied pressure, *J. Membr. Biol. 151*, 175-187.

26. Kung, C., Martinac, B., and Sukharev, S. (2010) Mechanosensitive channels in microbes, *Annu. Rev. Microbiol. 64*, 313-329.

27. Booth, I. R., Edwards, M. D., and Miller, S. (2003) Bacterial ion channels, *Biochemistry 42*, 10045-10053.

28. Blount, P., Sukharev, S. I., Moe, P. C., Schroeder, M. J., Guy, H. R., and Kung, C. (1996) Membrane topology and multimeric structure of a mechanosensitive channel protein of Escherichia coli, *EMBO J. 15*, 4798-4805.

29. Stokes, N. R., Murray, H. D., Subramaniam, C., Gourse, R. L., Louis, P., Bartlett, W., Miller, S., and Booth, I. R. (2003) A role for mechanosensitive channels in survival of stationary phase: regulation of channel expression by RpoS, *Proc Natl Acad Sci U S A 100*, 15959-15964.

30. Akitake, B., Anishkin, A., Liu, N., and Sukharev, S. (2007) Straightening and sequential buckling of the pore-lining helices define the gating cycle of the mechanosensitive channel MscS, *Manuscript Submitted*.

31. Steinbacher, S., Bass, R., Strop, P., and Rees, D. C. (2007) Structures of the Prokaryotic Mechanosensitive Channels MscL and MscS, *Current Topics in Membranes 58*.

32. Wang, W., Black, S. S., Edwards, M. D., Miller, S., Morrison, E. L., Bartlett, W., Dong, C., Naismith, J. H., and Booth, I. R. (2008) The structure of an open form of an E. coli mechanosensitive channel at 3.45 A resolution, *Science 321*, 1179-1183.

33. Vasquez, V., Sotomayor, M., Cordero-Morales, J., Schulten, K., and Perozo, E. (2008) A structural mechanism for MscS gating in lipid bilayers, *Science 321*, 1210-1214.

34. Vasquez, V., Sotomayor, M., Cortes, D. M., Roux, B., Schulten, K., and Perozo, E. (2008) Three-dimensional architecture of membrane-embedded MscS in the closed conformation, *J Mol Biol 378*, 55-70.

35. Anishkin, A., Akitake, B., and Sukharev, S. (2008) Characterization of the resting MscS: modeling and analysis of the closed bacterial mechanosensitive channel of small conductance, *Biophys J 94*, 1252-1266.

36. Anishkin, A., Kamaraju, K., and Sukharev, S. (2008) Mechanosensitive channel MscS in the open state: modeling of the transition, explicit simulations, and experimental measurements of conductance, *J Gen Physiol 132*, 67-83.

37. Belyy, V., Anishkin, A., Kamaraju, K., Liu, N., and Sukharev, S. (2010) The tension-transmitting 'clutch' in the mechanosensitive channel MscS, *Nat. Struct. Mol. Biol. 17*, 451-458.

38. Anishkin, A. and Sukharev, S. (2004) Water dynamics and dewetting transitions in the small mechanosensitive channel MscS, *Biophysical journal 86*, 2883-2895.

39. Anishkin, A. and Sukharev, S. (2004) Water dynamics and dewetting transitions in the small mechanosensitive channel MscS, *Biophys. J. 86*, 2883-2895.

40. Sotomayor, M., van der Straaten, T. A., Ravaioli, U., and Schulten, K. (2006) Electrostatic properties of the mechanosensitive channel of small conductance MscS, *Biophysical journal 90*, 3496-3510.

41. Anishkin, A., Akitake, B., and Sukharev, S. (2008) Characterization of the resting MscS: modeling and analysis of the closed bacterial mechanosensitive channel of small conductance, *Biophys. J. 94*, 1252-1266.

42. Grajkowski, W., Kubalski, A., and Koprowski, P. (2005) Surface changes of the mechanosensitive channel MscS upon its activation, inactivation, and closing, *Biophys. J. 88*, 3050-3059.

43. Koprowski, P., Grajkowski, W., Isacoff, E. Y., and Kubalski, A. (2010) Genetic screen for potassium leaky small mechanosensitive channels (MscS) in e. coli: recognition of cytoplasmic beta domain as a new gating element, *J Biol. Chem.*

44. Kamaraju, K., Belyy, V., Rowe, I., Anishkin, A., and Sukharev, S. (2011) The pathway and spatial scale for MscS inactivation, *Jouranal of General Physiology, in press*.

45. Edwards, M. D., Li, Y., Kim, S., Miller, S., Bartlett, W., Black, S., Dennison, S., Iscla, I., Blount, P., Bowie, J. U., and Booth, I. R. (2005) Pivotal role of the glycine-rich TM3 helix in gating the MscS mechanosensitive channel, *Nature structural & molecular biology 12*, 113-119.

46. Nomura, T., Sokabe, M., and Yoshimura, K. (2008) Interaction between the cytoplasmic and transmembrane domains of the mechanosensitive channel MscS, *Biophys J 94*, 1638-1645.

47. Edwards, M. D., Bartlett, W., and Booth, I. R. (2008) Pore mutations of the Escherichia coli MscS channel affect desensitization but not ionic preference, *Biophys. J 94*, 3003-3013.

48. Sotomayor, M. and Schulten, K. (2004) Molecular dynamics study of gating in the mechanosensitive channel of small conductance MscS, *Biophysical journal 87*, 3050-3065.

49. Machiyama, H., Tatsumi, H., and Sokabe, M. (2009) Structural Changes in the Cytoplasmic Domain of the Mechanosensitive Channel MscS During Opening, *Biophysical Journal 97*, 1048-1057.

50. Okada, K., Moe, P. C., and Blount, P. (2002) Functional design of bacterial mechanosensitive channels. Comparisons and contrasts illuminated by random mutagenesis, *The Journal of biological chemistry 277*, 27682-27688.

51. de, G. J. (1993) Osmotic behaviour and permeability properties of liposomes, *Chem. Phys. Lipids 64*, 187-196.

52. Beavis, A. D., Brannan, R. D., and Garlid, K. D. (1985) Swelling and contraction of the mitochondrial matrix. I. A structural interpretation of the relationship between light scattering and matrix volume, *J Biol. Chem. 260*, 13424-13433.

53. Koch, A. L. and Woeste, S. (1992) Elasticity of the sacculus of Escherichia coli, *J. Bacteriol. 174*, 4811-4819.

54. Kamaraju, K., Gottlieb, P. A., Sachs, F., and Sukharev, S. (2010) Effects of GsMTx4 on Bacterial Mechanosensitive Channels in Inside-Out Patches from Giant Spheroplasts, *Biophys. J 99*, 2870-2878.

55. Eze, M. O. and McElhaney, R. N. (1978) Stopped-flow spectrophotometric assay of glycerol permeation in Escherichia coli: applicability and limitations, *J Gen Microbiol. 105*, 233-242.

56. Hubert, J. F., Duchesne, L., Delamarche, C., Vaysse, A., Gueune, H., and Raguenes-Nicol, C. (2005) Pore selectivity analysis of an aquaglyceroporin by stopped-flow spectrophotometry on bacterial cell suspensions, *Biol. Cell 97*, 675-686.

57. Latimer, P. (1982) Light scattering and absorption as methods of studying cell population parameters, *Annu. Rev. Biophys. Bioeng. 11*, 129-150.

58. Shapovalov, G. and Lester, H. A. (2004) Gating transitions in bacterial ion channels measured at 3 micros resolution, *J. Gen. Physiol 124*, 151-161.

59. Sotomayor, M. and Schulten, K. (2004) Molecular dynamics study of gating in the mechanosensitive channel of small conductance MscS, *Biophys. J. 87*, 3050-3065.

60. Steinbacher, S., Bass, R., Strop, P., and Rees, D. C. (2007) Structures of the prokaryotic mechanosensitive channels MscL and MscS, *Mechanosensitive Ion Channels, Part A 58*, 1-24.

61. Akitake, B., Anishkin, A., Liu, N., and Sukharev, S. (2007) Straightening and sequential buckling of the pore-lining helices define the gating cycle of MscS, *Nat Struct Mol Biol 14*, 1141-1149.